Ab initio calculated XANES and XMCD spectra of Fe(II) phthalocyanine

Michael D. Kuz'min,[1] Roland Hayn,[2] and Vincent Oison[2]
[1]*Leibniz-Institut für Festkörper- und Werkstoffforschung, Postfach 270116, D-01171 Dresden, Germany*
[2]*Institut de Matériaux, Microélectronique et Nanosciences de Provence, Faculté de St. Jérôme, Université d'Aix-Marseille, UMR CNRS 6242, Case 142, F-13397 Marseille Cedex 20, France*
(Received 30 September 2008; revised manuscript received 21 November 2008; published 13 January 2009)

We report a density-functional calculation that predicts for iron(II) phthalocyanine (FePc) an unusual orbitally degenerate intermediate-spin ground state ^3E_g. The calculated Fe $L_{2,3}$ near-edge x-ray absorption spectrum agrees reasonably with experiment, whereas the presence of an unquenched orbital moment is corroborated by a recent discovery in α-FePc of a very large hyperfine field of *positive* sign [Filoti *et al.*, Phys. Rev. B **74**, 134420 (2006)]. It is suggested that the orbital moment of FePc should be observed more directly in x-ray magnetic circular dichroism experiments.

DOI: 10.1103/PhysRevB.79.024413 PACS number(s): 61.05.cj, 75.50.Xx

I. INTRODUCTION

The unfailing interest in metal phthalocyanines has two principal reasons: their numerous technological applications[1] and their similarity to the biological molecules chlorophyll and hemoglobin. The latter, in particular, is a close relative of iron(II) phthalocyanine (FePc). Over decades FePc has been extensively investigated by various experimental techniques,[2–5] including x-ray absorption.[6] Yet the numerous studies have failed to establish convincingly the ground state of the molecule, variously reported to be ^3E_g (Refs. 2 and 5) or $^3B_{2g}$ (Ref. 4) or $^3A_{2g}$ (Ref. 7) (a general consensus does seem to exist that $S=1$). Density-functional calculations have produced similarly contradictory predictions of $^3A_{2g}$ (Ref. 8) or $^3B_{2g}$ or ^3E_g (the latter two could not be decided between with certainty in Ref. 9, where they were found to lie "very close in calculated energy"). The proximity in energy may go some way toward explaining the conflicting experimental findings: these are related either to one of the two known polymorphs of FePc or to solutions. There is, however, little excuse for the calculations, all of which contemplate a single FePc molecule with a perfect D_{4h} symmetry and are supposed to produce consistent results.

Meanwhile, new experimental evidence has appeared of the ground state of the α polymorph being the orbitally degenerate ^3E_g. It is namely the discovery in α-FePc of an extraordinarily large hyperfine field,[10] whose unusual *positive sign* is an unambiguous indication of its orbital nature. An important implication of the orbital degeneracy is that the FePc molecules must be magnetically extremely anisotropic (Ising-type),[10] which makes them likely candidates for single-molecule information storage units. It is clear that experiments aimed at a more direct observation of an unquenched orbital moment of Fe^{2+} in FePc are both desirable and likely. An established technique for detecting orbital moments is x-ray magnetic circular dichroism (XMCD).[11] In anticipation of such experiments we have performed an *ab initio* calculation of the Fe $L_{2,3}$ near-edge x-ray absorption spectrum (XANES) and XMCD spectrum of FePc.

The XANES spectra were earlier calculated by Thole *et al.*[12] in a standard atomic approach taking account of the multiplet structure and of the ligand field, but disregarding hybridization. Such calculations have a rather limited power of prediction since they employ several fitting parameters that need to be conjectured. This includes the filling numbers for the electron shells of iron (assumed integer) as well as the entire set of ligand-field parameters.

The aim of this work is to make an *ab initio* prediction of XANES and XMCD spectra of FePc. We show the importance of hybridization effects for the interpretation of experimental data. The paper is structured as follows: Section II describes the $3d$ part of the electronic spectrum of Fe^{2+} at three different levels of approximation, arranged in order of ascending complexity. The calculation of the XANES and XMCD spectra is the subject matter of Sec. III, followed by a discussion in Sec. IV. Section V then concludes the paper.

II. ENERGY SPECTRUM OF Fe^{2+} IN FePc: THREE LEVELS OF APPROXIMATION

A. $3d$ states of iron in a ligand field of symmetry D_{4h}

At this simplest level of description, the five $3d$ orbitals of Fe^{2+} are split by the ligand field regardless of their occupation. The symmetry of a single FePc molecule is described by the point group D_{4h} and Fe^{2+} is situated in the center of the molecule. Any distortion of the ligand field due to stacking of individual molecules in chains is neglected. The individual $3d$ levels are three singlets and a doublet, labeled according to the irreducible representations of D_{4h}, see Fig. 1. Regarding the level pattern, only one feature appears essential at this stage: the b_{1g} orbital ($3d_{x^2-y^2}$) lies much higher in energy than the rest of the $3d$ states.

B. Ligand field+intra-atomic exchange on $3d^6$

Now each orbital is split according to spin, the spin-up (majority) states lying lower in energy, see Fig. 2. In the simplest approximation the exchange splitting is the same for all orbitals. It is essential that it exceeds the ligand-field splitting of the low-lying orbital levels, while being inferior to the gap separating the uppermost orbital b_{1g}. It is because of this very large ligand-field gap that the first Hund's rule is violated in FePc and the ground state has $S=1$ rather than $S=2$, as would be normally expected for Fe^{2+}. The fact that

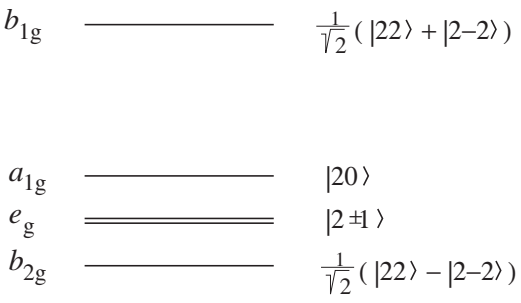

FIG. 1. Energy level pattern of the $3d$ shell of Fe^{2+} in FePc. The labels on the left are irreducible representations of the point group D_{4h}. The orbital eigenfunctions in the $|lm\rangle$ representation are on the right-hand side.

$S=1$ was derived from magnetic measurements some four decades ago.[2,4] The sequence of levels within the low-lying group of orbitals determines which ones of them are occupied in the minority-spin channel. The correct occupation scheme, shown in Fig. 2, was first proposed by Dale *et al.*[2] and later confirmed by the x-ray diffraction data of Coppens *et al.*[5] An important feature of this scheme is that the Fermi level passes through the middle of the orbital doublet e_g in the minority-spin channel. One implication of this is that the ground state of Fe^{2+} in FePc is orbitally degenerate. The weak spin-orbit coupling decides that one component of the doublet, whose orbital moment is parallel to the majority-spin direction ($\langle l_z\rangle=1$), should lie lower in energy and be filled, whereas the other component, with $\langle l_z\rangle=-1$, is vacant. The ground-state value for the entire Fe^{2+} is obviously $\langle L_z\rangle=1$.

C. Ligand field+intra-atomic exchange+hybridization

We have now reached a point whence we cannot advance any further without performing a full-scale electronic structure calculation. This means a clear departure from the largely qualitative and hypothesizing style of Secs. II A and II B. On the other hand, the results of this *parameter-free* calculation not only confirm the main conjectures stated above, but also provide additional quantitative information about the energy spectrum of FePc. This subsection should be therefore regarded as both a natural extension and a validation of our model approach.

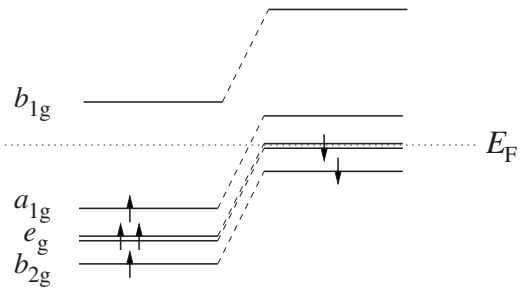

FIG. 2. The same spectrum as in Fig. 1, but split according to spin. The occupied component of the e_g doublet in the minority-spin channel is $|21\downarrow\rangle$, while the vacant component is $|2{-}1\downarrow\rangle$.

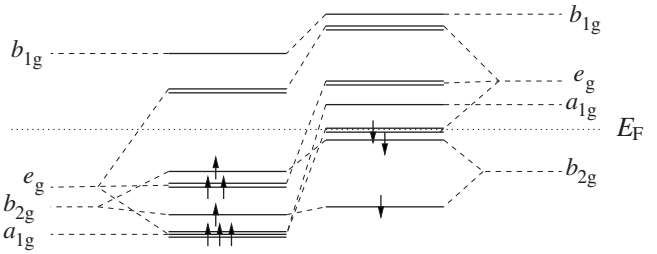

FIG. 3. Energy spectrum of FePc calculated *ab initio*. Only states with nonzero $3d$ weights around the Fermi level are shown. The energies are given in Table I. The spectrum resembles Fig. 2 but allows for hybridizaton (note the addition of several ligandlike states).

The density-functional calculations were spin polarized and carried out for a single FePc molecule. The exchange and correlation potential was taken in the generalized gradient approximation.[13] Version 2.0 of the SIESTA program was used.[14] We employed the norm-conserving pseudopotential of Troullier and Martins,[15] as well as a double-ζ polarized (DZP) basis set.[16]

Figure 3 displays the calculated energy spectrum in the vicinity of the Fermi level. One observes that the calculation, indeed, reproduces the fact that $S=1$. Moreover, the predicted level sequence in the minority-spin channel is the same as in Fig. 2. Namely, an e_g doublet lies at the Fermi level, an a_{1g} singlet is above E_F, and a b_{2g} singlet is below E_F. The level sequence in the majority-spin channel differs from that of Fig. 2. This difference, however, has no bearing on the physical properties since the same orbitals are filled in both pictures. Our results are therefore in agreement with the x-ray diffraction data of Coppens *et al.*[5] In the energy range relevant to XANES, i.e., several electronvolts above the Fermi level, only the doublet e_g level is seriously affected (split) by the hybridization with the ligand π orbitals. In the singlet states only the $3d$ content is slightly lowered (typically by a factor ~ 0.9).

In summary, allowance for the hybridization has surprisingly few implications for the XANES/XMCD calculations in comparison with the simple ionic picture of Fig. 2, mainly in the form of $3d$ weight factors and some additional lines due to splitting of energy levels (see Table I). The calculated energies of the unfilled $3d$ states are also listed in Table I. The additional empty e_g doublets will be seen to contribute only one extra line of significant intensity to XANES and nothing at all to the XMCD spectrum.

III. CALCULATION OF XANES AND XMCD SPECTRA

The absorption spectra, in arbitrary units, were calculated as follows:

$$\text{XANES} = \sum w_{3d}(I_+ + I_-)\,\delta(E - E_{3d} + E_{2p}), \qquad (1)$$

$$\text{XMCD} = \sum w_{3d}(I_+ - I_-)\,\delta(E - E_{3d} + E_{2p}). \qquad (2)$$

Here E_{3d} and w_{3d} are the calculated energies and $3d$ contents of the $3d$-like states (Table I), E_{2p} are the Fe $2p$ core-level

TABLE I. Energies and $3d$ weight factors of the levels displayed in Fig. 3. Negative energies correspond to fully occupied states. The $e_{g\downarrow}$ doublet situated at the Fermi level is half occupied: $|21\downarrow\rangle$ is filled, while $|2-1\downarrow\rangle$ is vacant.

	Majority spin (↑)		Minority spin (↓)	
Irrep. of D_{4h}	E_{3d} (eV)	w_{3d}	E_{3d} (eV)	w_{3d}
b_{1g}	1.96	0.830	2.99	0.912
e_g	1.06	0.041	2.84	0.031
	−1.28	0.396	1.24	0.230
	−2.57	0.431	0	0.625
b_{2g}	−0.21	0.867	−1.06	0.582
	−1.84	0.106	−2.10	0.415
a_{1g}	−2.57	0.801	0.72	0.914

energies taken from a standard source:[17] $E_{2p_{1/2}}=-719.9$ eV (the L_2 edge) and $E_{2p_{3/2}}=-706.8$ eV (the L_3 edge). The sums in Eqs. (1) and (2) run over all unoccupied $3d$-like states as well as over the two $2p_{1/2}$ and four $2p_{3/2}$ core states.

The transition intensities for the two circular polarization directions,

$$I_{\pm} = |\langle 3d|n_{\pm}|2p\rangle|^2, \tag{3}$$

were computed assuming the radial wave functions of all $2p$ as well as of all $3d$ states to be the same. In this approximation the radial parts of the matrix elements reduce to unimportant prefactors and can be omitted. The polarization operators $n_{\pm}$ are the cyclic components of the unit vector,[18]

$$n_{\pm} = \mp \frac{1}{\sqrt{2}}(n_x \pm i n_y) \tag{4}$$

defined in a coordinate system associated with the incident x-ray beam (see Fig. 4). For calculations it is more convenient to use n', defined in the molecular symmetry-related axes. The transformation formula is as follows:

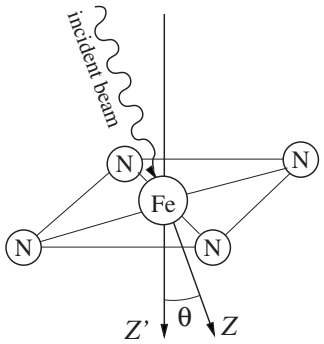

FIG. 4. Mutual orientation of the incident-beam-related and molecular symmetry-related (primed) coordinate axes.

$$n_{\pm} = \frac{1 \pm \cos\theta}{2} n'_{+} \mp \frac{\sin\theta}{\sqrt{2}} n'_{z} + \frac{1 \mp \cos\theta}{2} n'_{-}. \tag{5}$$

The matrix elements of the dipole transitions $2p$-$3d$ are given by Eqs. (13.2.13) of Ref. 18,

$$\langle 2m \pm 1|n'_{\pm}|1m\rangle = \sqrt{\frac{(2 \pm m)(3 \pm m)}{30}}, \tag{6}$$

$$\langle 2m|n'_{z}|1m\rangle = \sqrt{\frac{4-m^2}{15}}. \tag{7}$$

To use these equations, one needs to convert the $2p$ core states to the $|lmm_s\rangle$ representation and to take into account that the operators $n'_{\pm,z}$ are diagonal in m_s. There are two $2p_{1/2}$ states,

$$-\sqrt{\frac{1}{3}}|10\uparrow\rangle + \sqrt{\frac{2}{3}}|11\downarrow\rangle \quad \text{and} \quad \sqrt{\frac{1}{3}}|10\downarrow\rangle - \sqrt{\frac{2}{3}}|1-1\uparrow\rangle$$

and four $2p_{3/2}$ states,

$$|11\uparrow\rangle, |1-1\downarrow\rangle, \sqrt{\frac{2}{3}}|10\uparrow\rangle + \sqrt{\frac{1}{3}}|11\downarrow\rangle$$

and

TABLE II. Quantities relevant to Eqs. (1) and (2). $I_{\pm}^{(2,3)}$ are the squares of matrix elements, Eq. (3), the superscripts refer to the Fe absorption edges L_2 and L_3.

Final states	E_{3d} (eV)	w_{3d}	$I_{+}^{(3)}+I_{-}^{(3)}$	$I_{+}^{(2)}+I_{-}^{(2)}$	$I_{+}^{(3)}-I_{-}^{(3)}$	$I_{+}^{(2)}-I_{-}^{(2)}$
$b_{1g\downarrow}$	2.99	0.912	$\frac{2}{15}(1+\cos^2\theta)$	$\frac{1}{15}(1+\cos^2\theta)$	$-\frac{2}{15}\cos\theta$	$\frac{2}{15}\cos\theta$
$b_{1g\uparrow}$	1.96	0.830	$\frac{2}{15}(1+\cos^2\theta)$	$\frac{1}{15}(1+\cos^2\theta)$	$\frac{2}{15}\cos\theta$	$-\frac{2}{15}\cos\theta$
$e_{g\downarrow}$	2.84	0.031	$\frac{2}{15}(3-\cos^2\theta)$	$\frac{1}{15}(3-\cos^2\theta)$	0	0
$e_{g\downarrow}$	1.24	0.230	$\frac{2}{15}(3-\cos^2\theta)$	$\frac{1}{15}(3-\cos^2\theta)$	0	0
$e_{g\uparrow}$	1.06	0.041	$\frac{2}{15}(3-\cos^2\theta)$	$\frac{1}{15}(3-\cos^2\theta)$	0	0
$a_{1g\downarrow}$	0.72	0.914	$\frac{2}{45}(5-3\cos^2\theta)$	$\frac{1}{45}(5-3\cos^2\theta)$	$\frac{2}{45}\cos\theta$	$-\frac{2}{45}\cos\theta$
$\|2-1\downarrow\rangle$	0	0.625	$\frac{2}{15}$	$\frac{1}{30}(5-3\cos^2\theta)$	$-\frac{2}{15}\cos\theta$	$-\frac{1}{15}\cos\theta$

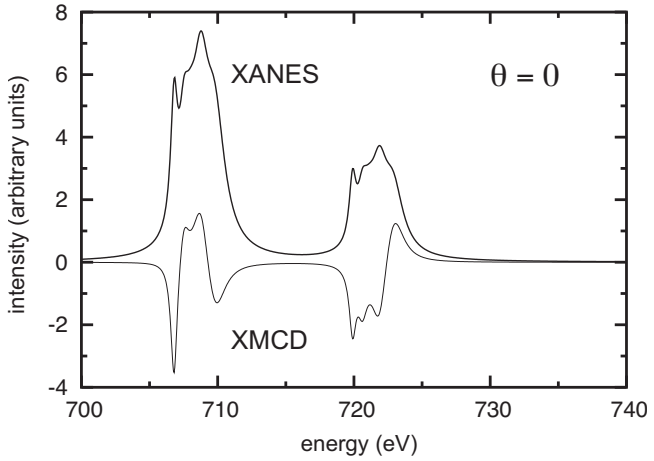

FIG. 5. Calculated XANES and XMCD spectra at $\theta=0$.

$$\sqrt{\frac{2}{3}}|10\downarrow\rangle + \sqrt{\frac{1}{3}}|1-1\uparrow\rangle.$$

Table II summarizes the resulting XANES and XMCD intensities, $I_+^{(i)} \pm I_-^{(i)}$, for the absorption edges L_i $(i=2,3)$ presented as functions of the incidence angle θ. The spectra generated for $\theta=0$ using the *ab initio* calculated $3d$ weight factors, energies, and transition intensities from Table II are presented in Fig. 5. The lines were of Lorentzian shape, the half width was assumed to depend on the energy of the final state linearly: $\Gamma=0.3\ \text{eV}+0.2(E_{3d}-E_F)$.

IV. DISCUSSION

Two considerations should be borne in mind regarding the data in Table II. First, the listed energies E_{3d} are differences of single-particle Kohn-Sham eigenvalues; they may inaccurately represent the actual one-particle excitation energies. Second, only the Fe $3d$-like states are shown, relevant to the Fe $L_{2,3}$ near-edge x-ray spectra (XANES, XMCD). Other spectroscopic techniques may not necessarily be selective to the Fe $3d$ states, then the generally more intense transitions into ligandlike states will dominate the spectra. A didactic example is the electron energy-loss spectrum (EELS) of FePc.[19] There, what can be assigned to a transition into the Fe $3d_{z^2}$ state $(a_{1g\downarrow})$ is a weak line at about 0.7 eV (predicted at 0.72 eV). This line is absent in the EELS of other metal phthalocyanines.[19] Yet, dominant in the EELS of phthalocyanines are transitions into ligand states, which are outside the scope of this work. Analyzing the formulas in Table II, one can make several observations specific to XANES or XMCD.

A. XANES $(I_+ + I_-)$

There are two groups of absorption lines, centered around ~708 and ~721 eV and corresponding to the L_3 and L_2 edges, respectively. The line intensities may depend on the incidence angle θ, nonetheless, each line of the L_3 group is twice as intense as its counterpart in L_2 at the same θ. Consequently, at any given θ the L_3 subspectrum has approximately the same shape, but is twice as high as the L_2 one.

The reason why the two subspectra are only approximately identical in shape is because there is one line (namely, the left-most one in each group) that does not follow the above rule. For this line the L_3/L_2 ratio at $\theta=0$ is the usual 2:1, however, at $\theta=90°$ it is 4:5. The anomalous line is not particularly intense, therefore, the above rule still holds approximately. The experiment does not seem to strongly disagree with this prediction—little more can be said at this point because of the poor resolution of the available XANES data.[6]

It is instructive to follow the evolution of the two lines on the low-energy flank of the subspectra. These lines are about 0.7 eV apart and correspond to $E_{3d}=0$ eV and $E_{3d}=0.72$ eV in Table II. Within the L_2 subspectrum, these two lines (unresolved in Fig. 5) are approximately equally intense at any θ, their intensity ratio being strictly independent of θ. The two left-most lines of the L_3 subspectrum behave quite differently: they are equally intense at $\theta=0$, but the second line (at $E_{3d}\approx 0.7$ eV) becomes 2.5 times higher as θ increases from 0 to 90°, while the intensity of the first left-most line of L_3 does not depend on θ at all.

The main body of XANES consists of three (not clearly resolved) lines. The higher-energy ones (at $E_{3d}=1.96$ and 2.99 eV) correspond to transitions into the b_{1g} states. Their intensities decrease with θ as $1+\cos^2\theta$. The low-energy member of the triplet, corresponding to a transition into an e_g state at $E_{3d}=1.24$ eV, is situated closer to the central line than the higher-energy one. Unlike the two b_{1g} lines, the e_g line gains in intensity according as θ grows.

Let us compare the combined intensities of the low-energy (doublet) line and the high-energy (triplet) line within the L_3 subspectrum. At $\theta=0$ the intensity ratio is about 0.3, however, it grows with θ, becoming close to 0.9 at $\theta=90°$. For random powder the substitution of 1/3 for $\cos^2\theta$ yields an intensity ratio of about 0.6. The experimental data[6] seem to bear out the latter prediction.

When going from the single molecule to a real material, the linewidths are expected to increase in a systematic way from left to right within each subspectrum. The underlying reason is that the FePc molecules in the sample are not isolated, but rather form periodic structures (chains). The molecular energy levels are therefore broadened into one-dimensional bands. The higher the molecular orbitals are situated on the energy scale, the more they overlap with the ones in the neighbor molecules. Hence the bandwidth—as well as the linewidth—should increase according as one moves along the energy axis from the Fermi level upwards. In addition, there is a general increase in the linewidth with energy due to lifetime effects.

B. XMCD $(I_+ - I_-)$

Both XMCD subspectra, L_2 and L_3, consist of four lines. Within the L_2 subspectrum, all the lines have the same sign except the highest-energy one, which is opposite in sign to the rest. In the L_3 subspectrum, the two outer lines have the same sign as most of the L_2 subspectrum, while the two central lines have the opposite sign.

The intensities of all XMCD lines have the same dependence on the incidence angle θ, $\propto \cos\theta$. Therefore, the shape of the XMCD spectrum does not depend on sample orientation with respect to the x-ray beam, even if the sample is textured (distributed over θ).

The intensity of each line in the L_3 subspectrum is equal in magnitude and opposite in sign to the corresponding line in the L_2 subspectrum. The only exception from this rule is the left-most lines of both subspectra, which have the same sign. These anomalous lines are the only contributors to the total integrated XMCD signal, proportional to the orbital moment.[11] Signs of the latter should thus be sought on the low-energy flank of the two XMCD subspectra.

V. CONCLUSION

We have presented a calculation of the $3d$ part of the electronic structure of FePc as well as derived thence XANES and XMCD spectra for the Fe $L_{2,3}$ edge. According to our calculations, the ground state of the molecule is ^3E_g, with $S=1$ and $|\langle L_z\rangle| \approx 1$. It is essential that hybridization is fully allowed for in the present calculations; this produces an extra absorption line 1.24 eV above the edge. The predicted XANES agrees with the available powder data[6] so it would be interesting in the future to compare it with higher-resolution data and/or with data obtained on oriented molecules. As regards XMCD, our predictions cannot yet be checked since no published XMCD spectra are available. It is however to be expected that such data will appear in the near future and will provide a test for our model and an answer to the important question, if indeed iron(II) phthalocyanine is endowed with a significant orbital moment.

ACKNOWLEDGMENTS

The authors are thankful to Juan Bartolomé for illuminating discussions. M.D.K. wishes to express his gratitude to the University of Aix-Marseille for the hospitality during his two successive stays in Marseille in 2008. Part of the work was carried out in Dresden and supported by the DFG under the Project No. RI 932/4-1.

[1] *Phthalocyanines: Properties and Applications*, edited by C. C. Leznoff and A. B. P. Lever (VCH, New York, 1996), Vol. 4.
[2] B. W. Dale, R. J. P. Williams, C. E. Johnson, and T. L. Thorp, J. Chem. Phys. **49**, 3441 (1968).
[3] B. W. Dale, R. J. P. Williams, P. R. Edwards, and C. E. Johnson, J. Chem. Phys. **49**, 3445 (1968).
[4] C. G. Barraclough, R. L. Martin, S. Mitra, and R. C. Sherwood, J. Chem. Phys. **53**, 1643 (1970).
[5] P. Coppens, L. Li, and N. J. Zhu, J. Am. Chem. Soc. **105**, 6173 (1983).
[6] E. E. Koch, Y. Jugnet, and F. J. Himpsel, Chem. Phys. Lett. **116**, 7 (1985).
[7] M. J. Stillman and A. J. Thomson, J. Chem. Soc., Faraday Trans. II **70**, 790 (1974).
[8] M.-S. Liao and S. Scheiner, J. Chem. Phys. **114**, 9780 (2001).
[9] P. A. Reynolds and B. N. Figgis, Inorg. Chem. **30**, 2294 (1991).
[10] G. Filoti, M. D. Kuz'min, and J. Bartolomé, Phys. Rev. B **74**, 134420 (2006).
[11] B. T. Thole, P. Carra, F. Sette, and G. van der Laan, Phys. Rev. Lett. **68**, 1943 (1992).
[12] B. T. Thole, G. van der Laan, and P. H. Butler, Chem. Phys. Lett. **149**, 295 (1988).
[13] J. P. Perdew, K. Burke, and M. Ernzerhof, Phys. Rev. Lett. **77**, 3865 (1996).
[14] J. M. Soler, E. Artacho, J. D. Gale, A. García, J. Junquera, P. Ordejón, and D. Sánchez-Portal, J. Phys.: Condens. Matter **14**, 2745 (2002).
[15] N. Troullier and J. L. Martins, Phys. Rev. B **43**, 1993 (1991).
[16] O. F. Sankey and D. J. Niklewski, Phys. Rev. B **40**, 3979 (1989).
[17] J. C. Fuggle and N. Mårtensson, J. Electron Spectrosc. Relat. Phenom. **21**, 275 (1980).
[18] D. A. Varshalovich, A. N. Moskalev, and V. K. Khersonskii, *Quantum theory of angular momentum* (World Scientific, Singapore, 1988).
[19] R. Kraus, A. König, and M. Knupfer *et al.* (unpublished).